Article

Model-Based Optimization Approach for PID Control of Pitch–Roll UAV Orientation

Orlando Arrieta [1,2,*], Daniel Campos [1], Javier Rico-Azagra [3], Montserrat Gil-Martínez [3,*], José D. Rojas [1,2] and Ramon Vilanova [2,*]

1   Instituto de Investigaciones en Ingeniería, Facultad de Ingeniería, Universidad de Costa Rica, San José 11501-2060, Costa Rica; danielantonio.campos@ucr.ac.cr (D.C.); jose.rojas_f@ucr.ac.cr (J.D.R.)
2   Departament de Telecomunicació i d'Enginyeria de Sistemes, Escola d'Enginyeria, Universitat Autònoma de Barcelona, Bellaterra, 08193 Barcelona, Spain
3   Control Engineering Research Group, Electrical Engineering Department, University of La Rioja, 26004 Logroño, Spain; javier.rico@unirioja.es
*   Correspondence: orlando.arrieta@ucr.ac.cr (O.A.); montse.gil@unirioja.es (M.G.-M.); ramon.vilanova@uab.cat (R.V.)

Abstract: This study focuses on the modeling and control optimization of the pitch–roll angles orientation in a quad-rotor UAV (unmanned aerial vehicle) drone system. To address the control challenge, PID (proportional–integral–derivative) controllers are used, which have been tuned through a model-based optimization approach. A non-linear model of the system is obtained and further validated experimentally. The model is implemented in Simulink to conduct model-based optimization. The controller design uses an IMC (internal model control) model-based approach to establish the initial parameters for a PID controller. In the subsequent design phase, a multiobjective approach is taken, incorporating weighted cost functions that account for IAE (integral absolute error) and ITAE (integral of time-weighted absolute error) forms, along with battery usage. The outcomes of this design are showcased through simulations and real-world platform testing.

Keywords: model-based optimization; multiobjective optimization; UAV system

MSC: 93B51

1. Introduction

Unmanned aerial vehicles (UAVs) are currently becoming increasingly popular in a wide range applications [1]. Although they were developed mainly for military purposes, it has recently become obvious that there are many other areas where UAVs might prove useful. In the field of agriculture, for example [2], they may be used for field observations or for chemical distribution. They can patrol over wide forest areas to monitor forest health [3], or they can be used for traffic observation in cities. Their potential applications in innumerable fields have led to their widespread use, and as a result, new challenges have arisen [4]. Additionally, the technological maturity of the sector has made it possible to configure ad hoc UAV equipment at a moderate cost [5–8], which has favored its use in training and research activities.

From a scientific and technical point of view, UAVs are multidisciplinary systems of special interest in engineering and, specifically, for the practice of control engineering [9,10]. In particular, controlling a multi-rotor-type UAV is a non-linear problem with six degrees of freedom (6-DoF) and with underactuation, especially when the thrusters cannot be reoriented [11,12]. For this reason, to address this complexity, a hierarchical control structure is commonly employed. The upper layers focus on positioning, while the lower layers handle orientation [13,14]. In turn, adequate control of position [15] makes the adequate tracking of trajectories possible [16]. However, the success of positioning is subject to adequate orientation control [17,18]. It is from this perspective that the present work focuses on this orientation problem.

UAV systems can be controlled using different methodologies, such as data-driven methodologies [19–21] or optimization techniques applied to proportional–integral–derivative (PID) controllers [22,23].

We use the experimental setup in [24] as our starting point. The test bench includes a fully equipped quad-rotor that rotates without displacement; these platforms are very popular for eliminating risky flight testing during controller design [25–27]. Its flight controller can be programmed from tools developed ad hoc in MATLAB-Simulink. A simulation environment allows us to prove control structures on a model that faithfully reproduces the behavior of the real system in order to establish a benchmark on control engineering [28]. This has been the core of the competition promoted by the Control Engineering Group of the Spanish Automatic Committee (CEA) [29]. The control strategy presented in this paper was an entry in the competition; it achieved the best result and therefore was the winner of the competition [30].

Considering this background, the objectives of this paper are twofold. We aim, on the one hand, to present a methodological application of our model-based controller design approach. On the other hand, we aim to exemplify controller tuning by successive refinement and improvement based on the optimization of PID controllers. This method of optimization is based on linear model approximation in the first stage in order to obtain suitable initial conditions for the next stage, where the optimization is carried out by taking a non-linear dynamics model as the basis. The results are tested on the experimental setup, therefore showing the validity of the overall approach. Equations for the flight patterns of the UAVs and non-linear dynamic equations are provided, and experimental adjustments to the experimental platform are also conducted.

The document is organized as follows. The next section describes our UAV system with a non-linear model. Then, in Section 3, the general framework for the control system is stated. Section 4 describes the procedure for the design of our controller and also describes the multi-objective problem we aim to optimize. We describe our implementation and validation processes on a real UAV platform in Section 5, and the paper ends in Section 6 with some conclusions and future work.

2. System Framework

The experimental setup and non-linear model considered in this work have been taken from [24]. In this study, a fully equipped quadrotor is affixed to a structure that permits unrestricted rotation without translation. The flight controller programming and real-time duplex transmission of commands and flight states to the remote pilot are facilitated through a set of MATLAB-Simulink tools. Moreover, a representative simulator is provided for testing purposes, making the configuration highly suitable for orientation control. The experimental setup is illustrated in Figure 1. In this section, the fist step is the reviewing of the non-linear model, followed by an experiment to validate the model and compare it against data generated using the experimental setup.

2.1. Non-Linear Model of the UAV

As mentioned, the main objective is to control the orientation of a multirotor UAV, characterized by the Euler angles ϕ, θ, and ψ. To maintain a fixed position and prevent displacement, a frame and two concentric rings are used, rotating on axes oriented $90°$, towards each other, allowing movement in ϕ and θ. Additionally, a mechanical locking system can be engaged to optionally restrict rotation in ψ. In Figure 2, the coordinate axes of the body system (X_B, Y_B, and Z_B) and the terrestrial inertial reference system (X_G, Y_G, and Z_G) are illustrated.
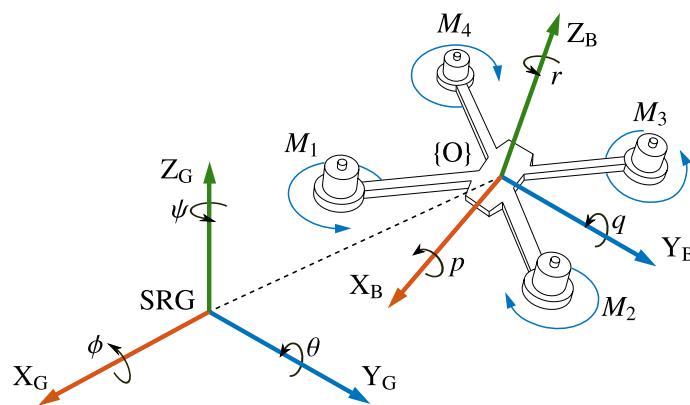
Figure 1. Experimental UAV setup.

Figure 2. Reference systems and main variables.

The system description is adapted from [24]. As expected, the propulsion forces align with the coordinates of the body system, leading to the multirotor UAV attaining speeds of p, q, and r along the X_B, Y_B, and Z_B coordinates, respectively, following the expressions

$$
\begin{aligned}
\dot{p} &= \frac{M_x - (I_z - I_y)qr}{I_x} \\
\dot{q} &= \frac{M_y - (I_x - I_z)pr}{I_y} \\
\dot{r} &= \frac{M_z - (I_y - I_x)pq}{I_z}
\end{aligned}
\tag{1}
$$

where the values I_x, I_y, and I_z represent the inertial values with respect to the axis, and the variables M_x, M_y, and M_z are the total moments about each axis, which are built as

$$
\begin{aligned}
M_x &= M_{\Gamma_x} + M_{r_x} + M_{\mu_x} + M_{g_x} \\
M_y &= M_{\Gamma_y} + M_{r_y} + M_{\mu_y} + M_{g_y} \\
M_z &= M_{\delta_z} + M_{r_z} + M_{\mu_z} + M_{g_z}
\end{aligned}
\tag{2}
$$

where M_g is the moment due to the gravitational force and is represented as

$$
\begin{aligned}
M_{g_x} &= -mgd\sin(\phi)\cos(\theta) \\
M_{g_y} &= -mgd\sin(\theta) \\
M_{g_z} &= 0
\end{aligned}
\tag{3}
$$

the m value denotes the mass of the multirotor UAV, d represents the distance from the center of gravity to the center of rotation $\{O\}$ along the Z_B axis, and g corresponds to the gravitational constant. At the same time, the values of M_r represent the gyroscopic moments given by a rotating mass,

$$
\begin{aligned}
M_{r_x} &= I_r(\omega_1 - \omega_2 + \omega_3 - \omega_4)q \\
M_{r_y} &= -I_r(\omega_1 - \omega_2 + \omega_3 - \omega_4)p \\
M_{r_z} &= I_r(\dot{\omega}_1 - \dot{\omega}_2 + \dot{\omega}_3 - \dot{\omega}_4)
\end{aligned}
\tag{4}
$$

where I_r stands for the inertia of each rotor and the ω refers to their respective turning speeds, which are directly influenced by the control signal. On the other hand, M_μ is equivalent to the moments due to static and viscous frictions in the mechanical couplings of the structure and is described as:

$$
\begin{aligned}
M_{\mu_x} &= \frac{-\mu_{C_x}p}{|p|} - \mu_x p \\
M_{\mu_y} &= \frac{-\mu_{C_y}q}{|q|} - \mu_y q \\
M_{\mu_z} &= \frac{-\mu_{C_z}r}{|r|} - \mu_z r
\end{aligned}
\tag{5}
$$

where the μ_C variables are the Coulomb friction coefficients and the μ variables are the viscous friction coefficients. The coefficients are combined to yield the moment M_Γ, which represents the total moment generated by the thrust forces of the propellers Γ. Additionally, the moment M_δ corresponds to the rotation around Z_B resulting from the algebraic combination of the drag moments δ. The mathematical expression describing these moments is shown as

$$
\begin{aligned}
M_{\Gamma_x} &= \frac{l(-\Gamma_1 + \Gamma_2 + \Gamma_3 - \Gamma_4)}{2\sqrt{2}} \\
M_{\Gamma_y} &= \frac{l(-\Gamma_1 - \Gamma_2 + \Gamma_3 + \Gamma_4)}{2\sqrt{2}} \\
M_{\delta_z} &= (-\delta_1 + \delta_2 - \delta_3 + \delta_4)
\end{aligned}
\tag{6}
$$

Table 1 shows the values of parameters in previous equations, which were obtained through measurements and experimentation. The variables Γ and δ, as well as the previously mentioned speeds ω, depend on the command signals of each motor in the form

$$
\begin{aligned}
\Gamma_i &= \frac{k_{\Gamma 2}(M_i - 1000)^2 k_i^2}{10^6} + \frac{k_{\Gamma 1}(M_i - 1000)k_i}{10^3} \\
\delta_i &= \frac{k_{\delta 2}(M_i - 1000)^2 k_i^2}{10^6} + \frac{k_{\delta 1}(M_i - 1000)k_i}{10^3} \\
\omega_i &= \frac{k_{\omega 1}(M_i - 1000)k_i}{10^3} + k_{\omega 0}
\end{aligned}
\tag{7}
$$

where M represents an RC PWM signal in between 1000μ and 2000μ. The coefficients k_Γ, k_δ, and k_ω vary with the supply voltage to the motors, as shown in Table 2; the experimental setup allows the variable voltage to emulate the battery charge level during flight. The

constants $k_1 = k_2 = 1$, $k_3 = 0.8$, and $k_4 = 0.86$ are due to the experimentally observed differences between rotors. Finally, the control signals of each motor are defined as

$$
\begin{aligned}
M_1 &= u_z - u_\phi - u_\theta - u_\psi \\
M_2 &= u_z + u_\phi - u_\theta + u_\psi \\
M_3 &= u_z + u_\phi + u_\theta - u_\psi \\
M_4 &= u_z - u_\phi + u_\theta + u_\psi
\end{aligned}
\tag{8}
$$

where u_ϕ, u_θ, and u_ψ represent the control actions for turning on each principal axis and u_z represents the control action for maintaining the altitude in hypothetical free flight. Then, taking $u_z = 1500\ \mu$ leaves a symmetric range of $\pm 500\ \mu$ to control the spins up to the saturation of the motor command. A mechanical lock on the structure optionally prevents yaw rotation when, as in this case, only attitude control is being performed. Consequently, u_ψ is forced to zero.

Table 1. Rotary body parameters.

	Value		Value
l	0.25 (m)	μ_{C_x}	0.006 (Nm/rad)
d	0.015 (m)	μ_{C_y}	0.006 (Nm/rad)
m	0.375 (kg)	μ_{C_z}	0.004 (Nm/rad)
I_x	0.00135 (kg^2)	μ_x	0.0015 (Nms/rad)
I_y	0.019 (kg^2)	μ_y	0.0015 (Nms/rad)
I_z	0.04 (kg^2)	μ_z	0.05 (Nms/rad)
I_r	1.05×10^{-6} (kg^2)		

Table 2. Propulsion system parameters.

	9 V	10 V	11 V	12 V
$k_{\Gamma 2}$	1.7796	1.2082	2.0105	2.0593
$k_{\Gamma 1}$	0.9554	1.1179	1.5707	1.9021
$k_{\delta 2}$	0.0238	0.0239	0.0318	0.0326
$k_{\delta 1}$	0.0202	0.0227	0.0266	0.0298
$k_{\omega 2}$	1445.8	1592.4	1762.9	1921.5
$k_{\omega 1}$	63.472	70.505	75.907	84.729

Having acquired this data, it becomes feasible to determine the velocities p, q, and r, concerning the control actions and the multirotor UAV position. The final step involves transforming the variables from the inertial reference system to the body system using quaternions. The rotational speed, expressed in quaternions in the reference system of the body corresponds to

$$
\begin{aligned}
\dot{q}_1 &= \frac{-q_2 p - q_3 q - q_4 r}{2} \\
\dot{q}_2 &= \frac{q_1 p - q_4 q + q_3 r}{2} \\
\dot{q}_3 &= \frac{q_4 p + q_1 q - q_2 r}{2} \\
\dot{q}_4 &= \frac{-q_3 p + q_2 q + q_1 r}{2}
\end{aligned}
\tag{9}
$$

from which we obtain $\mathbf{q} = [q_1\ q_2\ q_3\ q_4]^T$, a quaternion is employed to represent the orientation of the terrestrial reference system relative to the body's reference system. In the given equations, it is essential for the quaternion q to be normalized in the form $\mathbf{q} = \mathbf{q}/|\mathbf{q}|$

so that the conjugate quaternion $\mathbf{Q} = [Q_1 \; Q_2 \; Q_3 \; Q_4]^T = [q_1 \; -q_2 \; -q_3 \; -q_4]^T = \bar{\mathbf{q}}$ matches the inverse quaternion $\mathbf{q}^{-1}$. Thus, the Euler angles are calculated as

$$\begin{aligned}
\theta &= \arctan 2(2Q_1Q_2 + 2Q_3Q_4, 1 - 2Q_2^2 + 2Q_3^2) \\
\phi &= \arcsin(2Q_1Q_3 - 2Q_2Q_4) \\
\psi &= \arctan 2(2Q_1Q_4 + 2Q_2Q_3, 1 - 2Q_3^2 + 2Q_4^2)
\end{aligned} \tag{10}$$

2.2. Simulation Model and Validation

The above equations are integrated into the `UAV` block of the simulation model shown in Figure 3. This block contains, in addition to the UAV dynamics, a mathematical model of the IMU (inertial measurement unit) integrated in the flight controller and the estimation system used to determine the UAV attitude. This provides a representative model of the real system. It should be noted that the IMU model incorporates digital low-pass filters with a cut-off frequency of 20 Hz. These filters can significantly affect the system's behavior when the control bandwidth approaches the filter's cutoff frequency.

The non-linear model of the UAV is integrated into a feedback control structure; the control algorithms, as the one described in this paper, are implemented within the `control system` block, and the `set point` and `monitoring` blocks complete the structure of Figure 3. Further details on this simulation model can be found in [24]. Figure 4 shows one validation experiment that compares the real system and simulated outputs. Ignoring high-frequency unmodeled dynamics and noise, both results match quite well.

The complexity of the control system to be implemented is limited by the low-cost flight controller in the real platform. Thus, the computational load is constrained by a sampling frequency of 50 Hz, the precision is bounded by an 8-bit microcontroller resolution, and the limited memory and processing power recommend light control laws. PID-type controllers are clear candidates for this situation. The relevance and main contribution of this paper will thus be their off-line synthesis and optimization, which must lead to adequate performance in the nonlinear simulator and, finally, in the real test bench.

The non-linear model and the simulator are used hereinafter to construct a linear model-based controller design. Once the non-linear model is validated, the simulator allows us to take an optimal tuning approach to the two-degree-of-freedom PID controller parameters. The optimization algorithm interacts with the simulator to test and evaluate the current controller performance. The next section presents our controller design based on this non-linear model. The resulting controller is finally implemented and tested on the real platform.
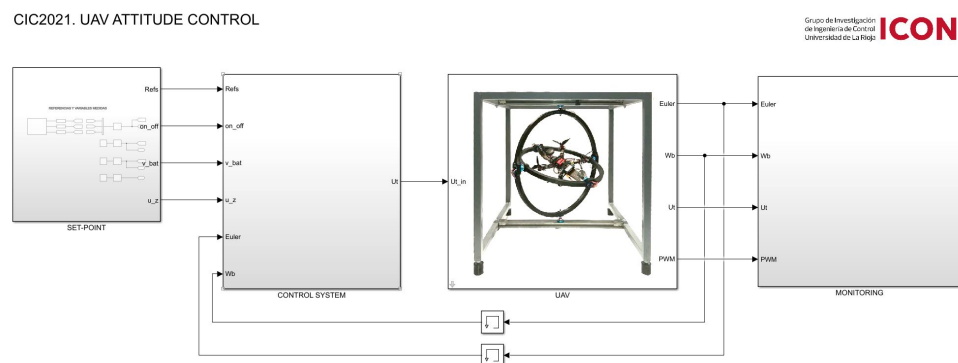

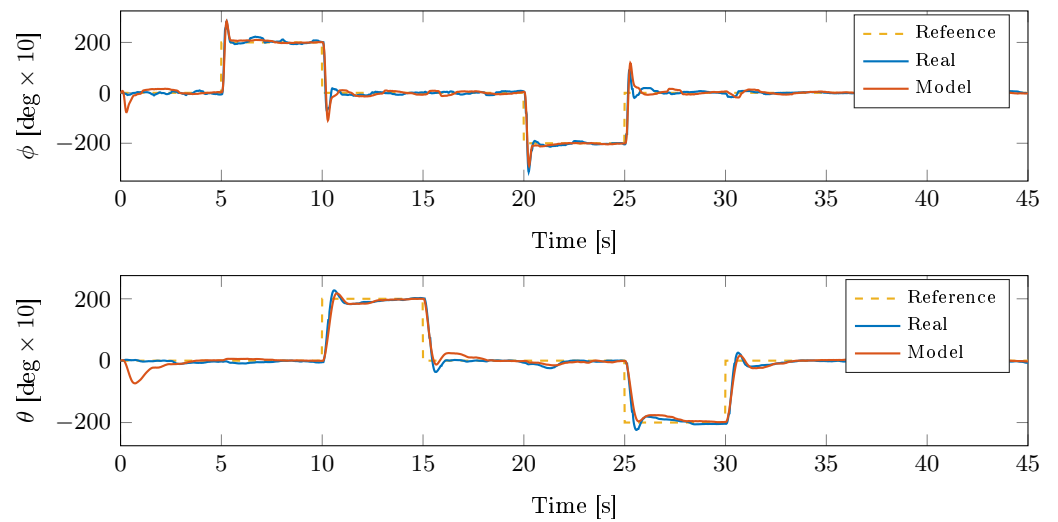**Figure 3.** Simulation model developed in MATLAB-Simulink.

Figure 4. Non-linear model validation with the experimental responses.

3. Control System

This section presents a description of the control system and describes how we approached the controller design process.

The considered control system is shown in Figure 5, whose variables are as below.
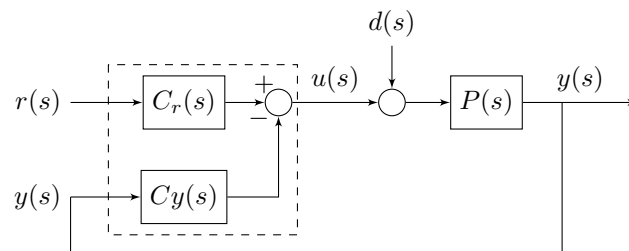

Figure 5. The considered control system structure.

- $y(s)$ is the process-controlled variable.
- $r(s)$ is the set point for the process output.
- $u(s)$ is the controller's output signal.
- $d(s)$ is the load disturbance of the system.

The transfer functions of the system are as follows. $P(s)$ is the controlled process, and the controller is a two degrees of freedom (2DoF) PID controller, with parameters of $\overline{p} = \begin{bmatrix} K_p, T_i, T_d, \beta \end{bmatrix}^T$. The controller is implemented in terms of its reference and output aspects $C_y(s)$ and $C_r(s)$ as

$$C_y(s) = K_p + \frac{K_i}{s} + \frac{K_d s}{0.1 K_d s + 1} \tag{11}$$

$$C_r(s) = \beta K_p + \frac{K_i}{s} \tag{12}$$

where

$$u(s) = C_r(s)r(s) - C_y(s)y(s) \tag{13}$$

For the UAV system, there are two control loops, one for each variable of interest. It is possible to delineate a relationship between the above general control structures with respect to the specific case where ϕ and θ (the roll and pitch angles, respectively) are the controlled variables, u_ϕ and u_θ are the control signals, r_ϕ and r_θ are the reference angles, and d is any disturbance input that can cause the angle to deviate from its reference. In free

flight, the main input disturbance is wind. Inside the structure that attaches the quadrotor, differences between the four rotors create important couplings between the roll and pitch control loops. These couplings are considered disturbance inputs for the control design.

Performance of the Control System

The effectiveness of a control system can be assessed by employing a cost function that relies on the error, defined as the difference between the desired value r (set point) and the current value of the controlled variable y (the system's output). Certainly, when time increases, the error becomes larger and longer, and therefore, the system's performance tends to degrade. As a measure of evaluating the controller's performance, a widely used reference is a functional based on the integral of the error, like the integral absolute error (IAE) or the integral time-weighted absolute error ($ITAE$), which also considers the duration of the error over time.

There is another index that measures the effort of the control action, which is computed as the integral of the absolute value for the variation of the control signal ($IAVU$). For this index, when a higher value is obtained, it indicates that the control action varies more abruptly.

The formulation of the indices is stated as

$$IAE = \int_0^{t_f} |r(t) - y(t)| dt \tag{14}$$

$$ITAE = \int_0^{t_f} t|r(t) - y(t)| dt \tag{15}$$

$$IAVU = \int_0^{t_f} \left| \frac{du(t)}{dt} \right| dt \tag{16}$$

where they can be measured for changes in the set point (servo control) or in the load disturbance (regulatory control).

The global evaluation of performance combines the previous indices as

$$J_o = w_1 IAE + w_2 ITAE + w_3 IAVU \tag{17}$$

with the weighting factors $w_1 = w_2 = 0.4$ and $w_3 = 0.2$, which evaluate the error indices (IAE and $ITAE$) and the control action ($IAUV$). These weighting factors are given by the benchmark from [24].

Then, the controller tuning design can be solved as an optimization problem that can be stated as

$$J_o^o \doteq \min_{K_p, K_i, K_d, \beta} J_o \tag{18}$$

where J_o^o is the achieved optimal value for the index J_o (17).

4. Controller Design

The design and tuning of the PID controller was carried out in three steps. First of all, a second-order linear model approximation for each channel (roll (ϕ) and pitch (θ)) was identified using data obtained from the non-linear simulator. The control system's design was established from those models using the internal model control (IMC) technique and then improved by optimization algorithms. Finally, the controllers were optimized using the non-linear simulation model.

4.1. Model Identification

The purpose of the identification of the obtained models was to help determine the initial controllers that were taken as initial conditions by the optimization algorithm.

Since the model identification was conducted through open-loop experiments, our first step was to determine the control actions that stabilized the UAV at roll (ϕ) and pitch

(θ) angles of zero. The rotor asymmetries required the non-null actions of $u_\phi = 9.2$ μs and $u_\theta = 47$ μs.

Once a stable orientation was achieved, three tests were carried out in open-loop conditions in order to obtain the process responses to step inputs for the following conditions:

- The response for ϕ to a step increment of 15 μs at u_ϕ;
- The response for θ to a step increment of 15 μs at u_θ.

Some measures were taken from each response, including the maximum value for the output (y_p) and the time of its occurrence (t_p), as well as the steady-state value for the system's output (y_{ss}). With all this information, the models were identified using the form

$$P(s) \approx P_m(s) = \frac{K\omega_n^2}{s^2 + 2\xi\omega_n s + \omega_n^2} \tag{19}$$

where $P_m(s)$ is the identified model of $P(s)$, where K represents the static gain, ξ indicates the damping ratio, and ω_n is the natural frequency.

From Model (19), we can see that it is well-known that the overshoot of the response (M_p) can be calculated as

$$M_p = \frac{y_p - y_{ss}}{y_{ss}} \tag{20}$$

and using the following relationships, the model parameters are:

$$\xi = \sqrt{\frac{ln(M_p)^2}{\pi^2 + ln(M_p)^2}} \tag{21}$$

$$\omega_n = \frac{\pi}{t_p\sqrt{1 - \xi^2}} \tag{22}$$

The results of these performed identifications allow us to obtain the parameters of Equations (21) and (22), which are systematized in Table 3. The open-loop responses for each angle (for the real system and model) are shown in Figure 6.
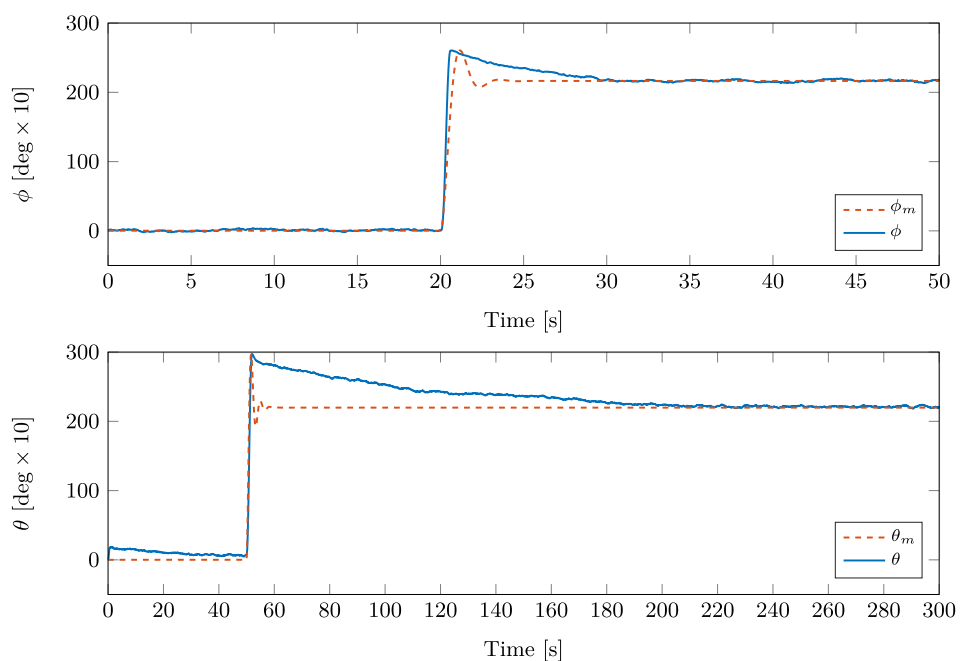

Figure 6. Real system and model responses for roll and pitch to a 15 μs step in their control actions.

Table 3. Parameters for the second-order model $P_m(s)$.

	P_ϕ	P_θ
K	14.400	14.700
ω_n	3.000	2.000
ξ	0.452	0.316

Once the models were obtained, the controller was designed following the below steps:

- The PID controller was designed using the internal model controller (IMC) approach in (23).
- The PID-IMC's tuning was improved by analyzing the multiobjective problem (18) on the basis of the identified linear models in Table 3.
- A second refinement of the controller's parameters was performed using the non-linear model presented in Section 2 as a simulation model for the optimization of Problem (18).

The final, third controller was tested on the real equipment. The following subsections will describe the detailed processes of each of the design steps.

4.2. Initial IMC Controller

An initial PID controller was designed from the identified second-order models using the IMC method. The expression for this controller is

$$C_y(s) = \frac{1}{T_c s}\left[\frac{1}{P_m(s)}\right] \tag{23}$$

where T_c is the desired closed-loop time constant. Note that the resulting structure for Equation (23) is the same as for Equation (11).

Taking into consideration that the purpose of this IMC controller is to serve as the starting point to be improved by means of the optimization procedure in the next step, the tuning value of T_c for each channel was selected in such a way that they provided the fastest closed-loop responses (in fact, T_c is the desired closed-loop time constant) while preserving stability (or, in other words, without the system becoming unstable). The resulting values are $T_c = 0.16$ for ϕ and $T_c = 0.06$ for θ. This represents a closed-loop system bandwidth between 8 and 10 times that of the corresponding open loop.

The parameters of the tuned controllers C_ϕ and C_θ for each controlled variable, following Equation (13), are shown in Table 4. In this case, the set-point weighting factor was set to the default value of $\beta = 1$.

Table 4. Controller parameters for the IMC method.

	IMC	
	C_ϕ	C_θ
K_p	0.039	0.358
K_i	0.129	1.134
K_d	0.014	0.283
β	1	1

In order to see the initial performance of the controllers using the IMC method at each channel (roll (ϕ) and pitch (θ)), a test was conducted with controllers from Table 4. The results are shown in Figure 7, and the performance indices IAE, $ITAE$, and $IAUV$, as well as the global index performance J_o, are displayed in Table 5. They were computed by applying Equation (14) to (17).
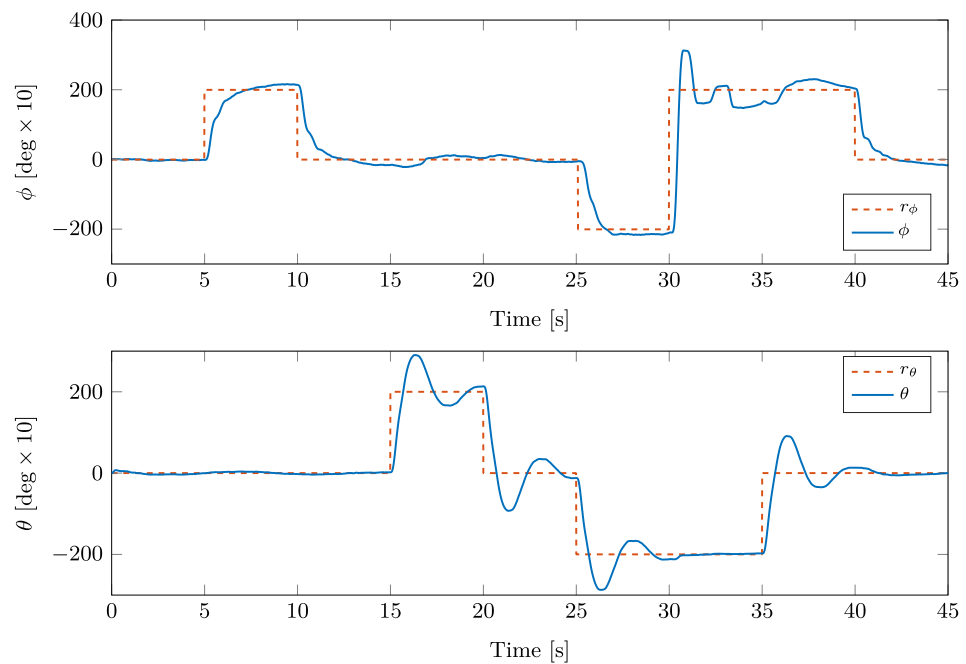
Figure 7. Roll and pitch responses in reference tracking using the IMC controller.

Table 5. Performance indices for the IMC controllers.

	IAE	ITAE	IAVU	J_o
Roll (ϕ)	2.996	3.365	0.059	2.556
Pitch (θ)	2.437	3.967	0.333	2.628

As can be seen, even the reference is followed with coarse precision. Thus, it is possible to take this controller (IMC) as initial conditions to be improved as one of the main purposes of the paper.

4.3. Improved Optimized Controller

The optimal controller's parameters were determined using the MATLAB function *fminsearch*. The initial controllers were obtained through the IMC method (as shown in Table 4) and the optimization process is using the linear models provided in Table 3.

In this manner, the optimization process runs smoother and faster. The function to be optimized is J_o (17). The parameters obtained through the optimization problem in Equation (18) are shown in Table 6.

Table 6. Controller parameters for optimization with the linear model (L).

	Optimal (L)	
	C_ϕ	C_θ
K_p	0.129	0.803
K_i	0.004	0.403
K_d	0.024	0.159
β	1.519	0.984

The responses for the controlled-variable roll (ϕ) and pitch (θ) using the optimized PID controllers shown in Table 6 are shown in Figure 8, and our evaluation of their performance is shown in Table 7.

The proposed control strategy not only performs well in tracking reference r changes but also in correcting any other cause of output deviations, i.e., compensating for disturbance inputs. In the present case, the experimentally observed differences between the

rotors generate couplings between the roll and pitch control loops, which act as disturbance inputs. These couplings have more effect on the axis with less inertia (Table 1 concludes $I_x \ll I_y$). Consequently, Figure 8 shows how the roll (ϕ) angle (Y_B-axis rotation) hardly deviates when the pitch reference (r_θ) changes, while the dynamic recovery of the pitch (θ) angle (X_B-axis rotation) is fast but visible after a change in the roll reference (r_ϕ).

In addition, it is possible to see that the optimized controllers achieved from the linear model provide a significant improvement in the performance evaluation by comparing the data from Tables 5 and 7.
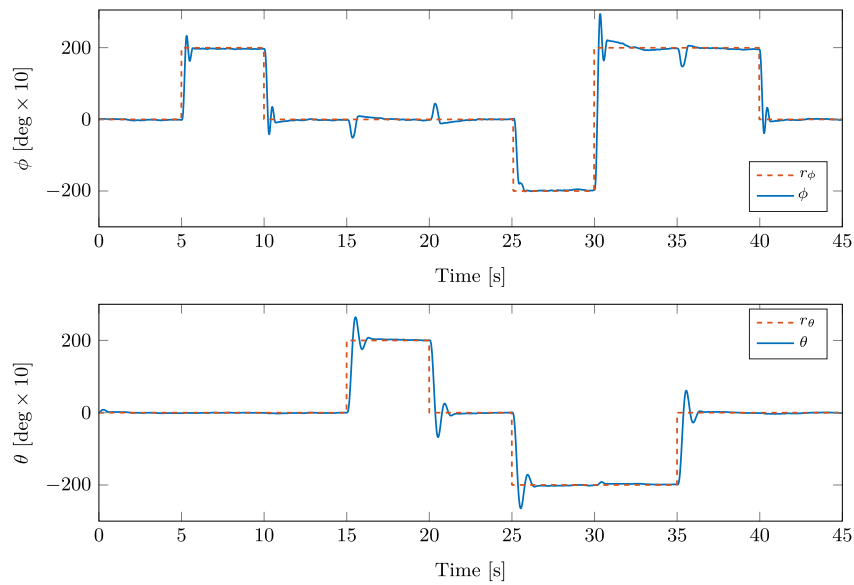

Figure 8. Roll and pitch responses in reference tracking using the optimized (L) controller.

Table 7. Performance indices for the optimized (L) controllers.

	IAE	ITAE	IAVU	J_o
Roll (ϕ)	1.063	0.781	0.174	0.772
Pitch (θ)	0.894	0.525	0.410	0.650

4.4. Optimized Controller for the Non-Linear Model

In this step, the tuning of the controller consisted of the optimization of Equation (17) by means of Equation (18) and using the MATLAB function *fminsearch* . However, we also considered the non-linear model (NL) plant described in Section 2 in this process. The parameters in Table 6 were used as initial controllers for optimization.

The controller parameters achieved from the above for the current optimization are shown in Table 8.

Table 8. Controller parameters for optimization with the non-linear model (NL).

	Optimal (NL)	
	C_ϕ	C_θ
K_p	0.137	0.936
K_i	0.149	0.803
K_d	0.028	0.234
β	1.273	0.826

The control structure of Figure 5 and controller parameters of Table 8 were implemented inside the `control system` block of the non-linear simulator in Figure 3. Consequently, Figure 9 shows the reference tracking and coupling compensation capabilities for the roll (ϕ) and pitch (θ) angles. Additionally, Table 9 shows the values of the performance indices for this case.

It is important to highlight that conducting the optimization directly with the non-linear model of the system, rather than using the identified linear model, resulted in a substantial improvement in performance. This can be checked by comparing the values in Tables 7 and 9.
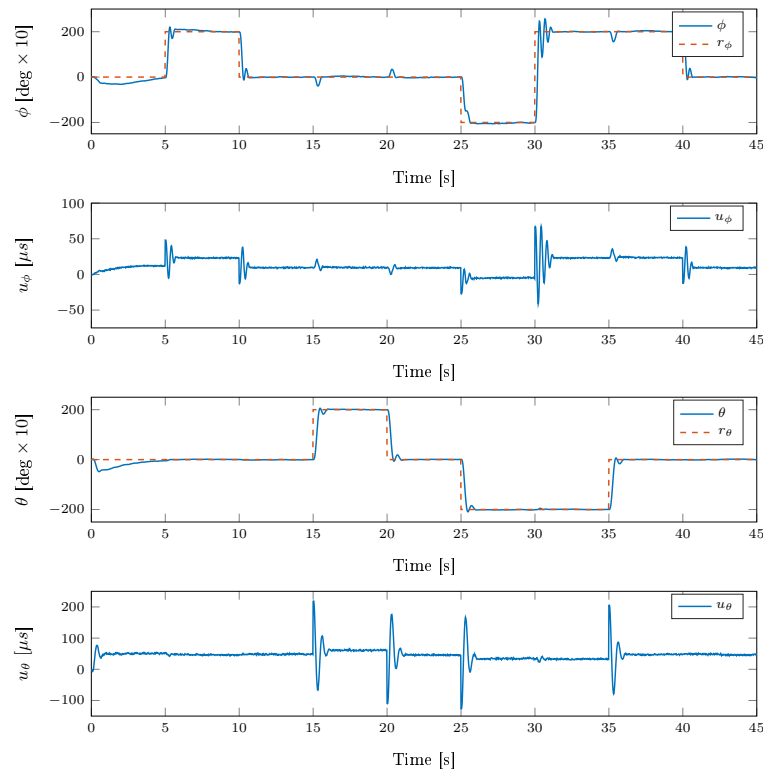

Figure 9. Simulated non-linear (NL) responses of the final optimized controller for roll (ϕ) and pitch (θ) rotations.

Table 9. Performance indices for the optimized (NL) controllers.

	IAE	ITAE	IAVU	J_o
Roll (ϕ)	0.958	0.609	0.222	0.671
Pitch (θ)	0.646	0.317	0.498	0.484

5. Implementation and Validation Results

The final controllers obtained in Section 4.4 were implemented in the real platform of the UAV system. This was a part of a competition promoted by the Control Engineering Group of the Spanish Automatic Committee (CEA) [29]. The three finalist designs are labeled T1, T2 and T3, with the latter being the one proposed in this work.

As a validation test, the controllers were evaluated using different power supply voltages in the UAV system. Experiments were conducted for battery voltages of 10 V, 11 V, and 12 V. This was performed with the aim of verifying how the state of the battery charge affects the behavior of the UAV when different supply voltages are used.

Table 10 shows the value for the performance indices for the roll (ϕ) and pitch (θ) angles for each of the power supply voltages. Moreover, the control system responses for the case of 11V are shown in Figure 10, where, in addition to the signal for each angle (ϕ and θ), the speeds reached by the multi-rotor UAVs (p and q) are shown, as well as the control signals (u_ϕ and u_θ). A video of this experiment in the real platform can be seen in [30].

Table 10. Performance evaluation and comparison for the UAV system.

Control Design	[V]	Roll (ϕ)			
		IAE	ITAE	IAVU	J_o^ϕ
T1	10	1.268	1.000	0.200	0.947
	11	1.309	1.261	0.245	1.077
	12	1.591	2.082	0.389	1.547
T2	10	1.523	2.327	0.077	1.556
	11	1.526	1.754	0.092	1.327
	12	1.498	1.897	0.129	1.384
T3	10	1.405	1.290	0.179	1.114
	11	1.408	1.647	0.232	1.268
	12	1.384	2.233	0.380	1.523
Control Design	[V]	Pitch (θ)			
		IAE	ITAE	IAVU	J_o^ϕ
T1	10	1.280	1.937	0.304	1.348
	11	1.094	1.380	0.309	1.056
	12	0.973	1.049	0.503	0.905
T2	10	1.740	2.264	0.118	1.625
	11	1.670	2.565	0.159	1.726
	12	1.511	1.943	0.185	1.418
T3	10	0.867	0.735	0.456	0.732
	11	0.818	0.677	0.586	0.715
	12	0.780	0.641	0.759	0.720

In order to have more usable information, , it is possible to calculate an averages for the experiments for each control design from the data of Table 10, as follows:

$$\overline{J_o} = \frac{J_o^\phi + J_o^\theta}{2} \tag{24}$$

Moreover, a general global index $\overline{J_O}$ can be computed as an average of each of the tests. All these calculations are provided by Table 11, where it is possible to see that the proposed multi-objective PID design is the best and gives the lowest value for $\overline{J_O}$.

Table 11. Average values for the performance index using the UAV system.

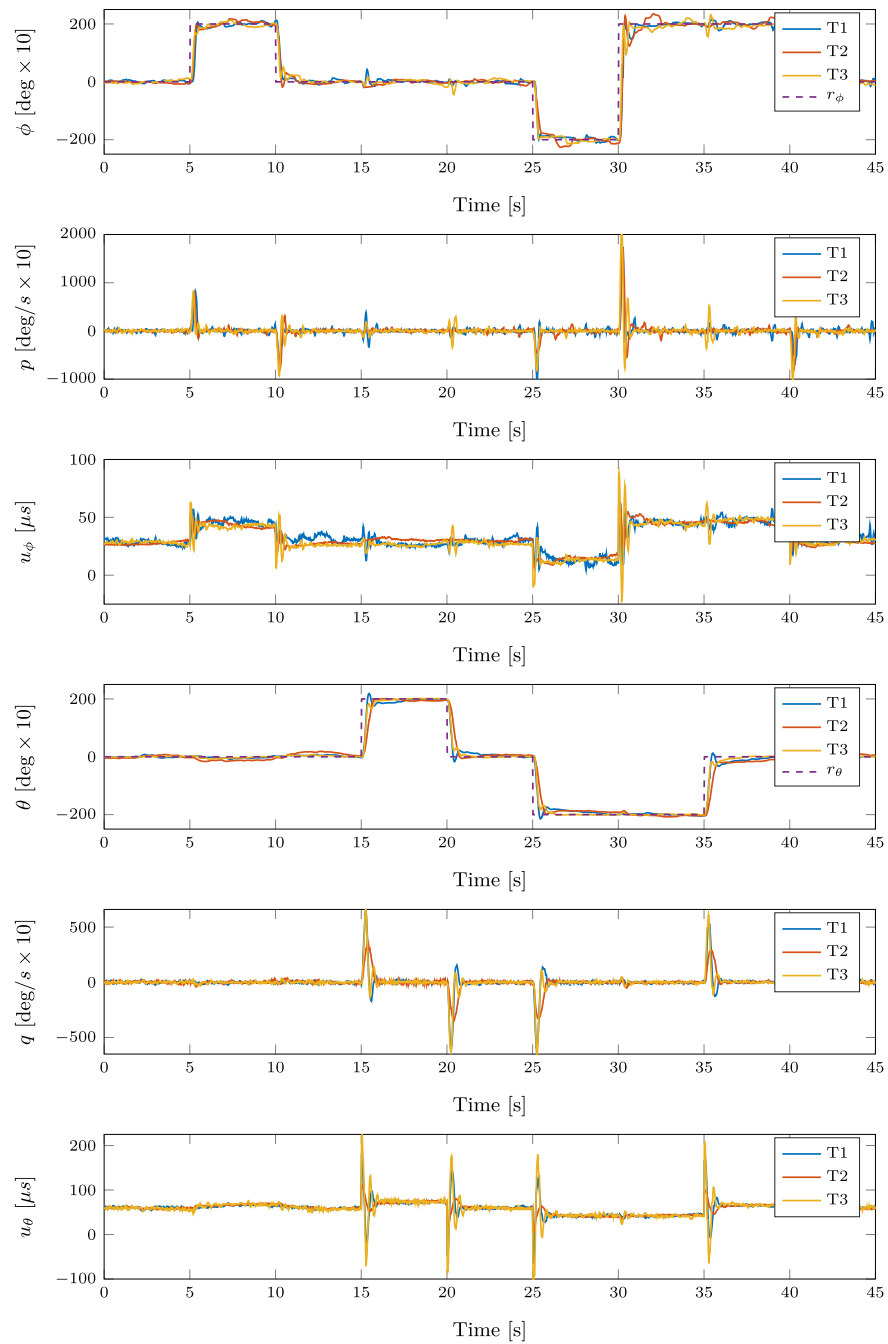| Control Design	[V]	$\overline{J_o} = \frac{J_o^\phi + J_o^\theta}{2}$	$\overline{J_O}$
T1	10	1.148	
	11	1.066	1.147
	12	1.228	
T2	10	1.590	
	11	1.526	1.506
	12	1.401	
T3	10	0.923	
	11	0.992	1.012
	12	1.121	

Figure 10. UAV control system responses for roll and pitch rotations with 11 V battery charge.

6. Conclusions

This study focuses on addressing the pitch–roll angle orientation in a quadrotor UAV drone system. The control approach involves the use of PID controllers and tuning them through multi-objective optimization. The UAV system is represented by a non-linear model, wit its respective interactions. The experimental setup successfully validates the non-linear model, as it aligns with the conducted control experiment.

The proposed control design for the PID controllers shows good performance for the system, providing low values for the indices *IAE, ITAE, IAUV,* and the global *J₀* and improving the results of the multi-objective optimization problem.

Three different control designs were implemented in the real UAV platform. Ultimately, the control method proposed in this paper offered the best performance for the system compared to the other two methods.

Our future work will involve the inclusion of a third variable to control, the angle ψ, which adds more complexity to the problem since the drag forces acting on the rotors are much smaller than their thrust forces. Other improvements will include a robustness analysis to take into account the battery discharge, which reduces rotor force. Finally, it will be beneficial to extend our validations to a free-flight experiment from the confinement platform once altitude control is included.

Author Contributions: Conceptualization, O.A., J.D.R. and R.V.; data curation, D.C., J.D.R. and J.R.-A.; formal analysis, O.A., J.D.R., M.G.-M. and R.V.; funding acquisition, O.A. and R.V.; investigation, O.A., D.C., J.R.-A. and R.V.; methodology, D.C., J.D.R. and R.V.; software, D.C. and J.R.-A.; project administration, O.A.; resources, O.A., J.D.R. and M.G.-M.; supervision, M.G.-M. and R.V.; validation, J.D.R., M.G.-M. and R.V.; visualization, J.R.-A.; writing—original draft, O.A.; writing—review and editing, M.G.-M. and R.V. All authors have read and agreed to the published version of the manuscript.

Data Availability Statement: Not applicable.

Conflicts of Interest: The authors declare no conflict of interest.

References

1. Mohsan, S.A.H.; Khan, M.A.; Noor, F.; Ullah, I.; Alsharif, M.H. Towards the Unmanned Aerial Vehicles (UAVs): A Comprehensive Review. *Drones* **2022**, *6*, 147. [CrossRef]
2. Rejeb, A.; Abdollahi, A.; Rejeb, K.; Treiblmaier, H. Drones in agriculture: A review and bibliometric analysis. *Comput. Electron. Agric.* **2022**, *198*, 107017. [CrossRef]
3. Ecke, S.; Dempewolf, J.; Frey, J.; Schwaller, A.; Endres, E.; Klemmt, H.J.; Tiede, D.; Seifert, T. UAV-Based Forest Health Monitoring: A Systematic Review. *Remote Sens.* **2022**, *14*, 3205. [CrossRef]
4. Shakhatreh, H.; Sawalmeh, A.H.; Al-Fuqaha, A.; Dou, Z.; Almaita, E.; Khalil, I.; Othman, N.S.; Khreishah, A.; Guizani, M. Unmanned Aerial Vehicles (UAVs): A Survey on Civil Applications and Key Research Challenges. *IEEE Access* **2019**, *7*, 48572–48634. [CrossRef]
5. Madridano, A.; Campos, S.; Al-Kaff, A.; García, F.; Martín, D.; Escalera, A. Unmanned aerial vehicle for fire surveillance and monitoring. *Rev. Iberoam. Autom. Inform. Ind.* **2020**, *17*, 254–263. [CrossRef]
6. Kangunde, V.; Jamisola, R.S.; Theophilus, E.K. A review on drones controlled in real-time. *Int. J. Dyn. Control* **2021**, *9*, 1832–1846. [CrossRef]
7. Bigazzi, L.; Gherardini, S.; Innocenti, G.; Basso, M. Development of Non Expensive Technologies for Precise Maneuvering of Completely Autonomous Unmanned Aerial Vehicles. *Sensors* **2021**, *21*, 391. [CrossRef]
8. Rico, R.; Rico-Azagra, J.; Gil-Martínez, M. Hardware and RTOS Design of a Flight Controller for Professional Applications. *IEEE Access* **2022**, *10*, 134870–134883. [CrossRef]
9. Khan, S.; Jaffery, M.H.; Hanif, A.; Asif, M.R. Teaching Tool for a Control Systems Laboratory Using a Quadrotor as a Plant in MATLAB. *IEEE Trans. Educ.* **2017**, *60*, 249–256. [CrossRef]
10. Gonzalez-Vargas, A.M.; Serna-Ramirez, J.M.; Fory-Aguirre, C.; Ojeda-Misses, A.; Cardona-Ordoñez, J.M.; Tomba-Andrade, J.; Soria-Lopez, A. A low-cost, free-software platform with hard real-time performance for control engineering education. *Comput. Appl. Eng. Educ.* **2019**, *27*, 406–418. [CrossRef]
11. Zhang, X.; Li, X.; Wang, K.; Lu, Y. A Survey of Modelling and Identification of Quadrotor Robot. *Abstr. Appl. Anal.* **2014**, *2014*, 320526. [CrossRef]
12. Shraim, H.; Awada, A.; Youness, R. A survey on quadrotors: Configurations, modeling and identification, control, collision avoidance, fault diagnosis and tolerant control. *IEEE Aerosp. Electron. Syst. Mag.* **2018**, *33*, 14–33. [CrossRef]
13. Nascimento, T.P.; Saska, M. Position and attitude control of multi-rotor aerial vehicles: A survey. *Annu. Rev. Control.* **2019**, *48*, 129–146. .: 10.1016/j.arcontrol.2019.08.004. [CrossRef]
14. Marshall, J.A.; Sun, W.; L'Afflitto, A. A survey of guidance, navigation, and control systems for autonomous multi-rotor small unmanned aerial systems. *Annu. Rev. Control.* **2021**, *52*, 390–427. [CrossRef]
15. Gil-Martinez, M.; Rico-Azagra, J. Multi-rotor robust trajectory tracking. In Proceedings of the 2015 23rd Mediterranean Conference on Control and Automation (MED), Torremolinos, Spain, 16–19 June 2015; pp. 865–870. [CrossRef]

16. Rubí, B.; Pérez, R.; Morcego, B. A Survey of Path Following Control Strategies for UAVs Focused on Quadrotors. *J. Intell. Robot. Syst.* **2020**, *98*, 241–265. [CrossRef]

17. Lotufo, M.A.; Colangelo, L.; Perez-Montenegro, C.; Canuto, E.; Novara, C. UAV quadrotor attitude control: An ADRC-EMC combined approach. *Control. Eng. Pract.* **2019**, *84*, 13–22. [CrossRef]

18. Chen, Y.; Zhang, G.; Zhuang, Y.; Hu, H. Autonomous Flight Control for Multi-Rotor UAVs Flying at Low Altitude. *IEEE Access* **2019**, *7*, 42614–42625. [CrossRef]

19. Invernizzi, D.; Panizza, P.; Riccardi, F.; Formentin, S.; Lovera, M. Data-driven attitude control law of a variable-pitch quadrotor: A comparison study. *IFAC-PapersOnLine* **2016**, *49*, 236–241. [CrossRef]

20. Capocchiano, S.; Panizza, P.; Invernizzi, D.; Lovera, M. Closed-loop data-driven attitude control design for a multirotor UAV. In Proceedings of the IEEE Conference on Control Technology and Applications (CCTA), Copenhagen, Denmark, 21–24 August 2018; pp. 153–158.

21. Zangarini, A.; Invernizzi, D.; Panizza, P.; Lovera, M. Closed-loop MIMO data-driven attitude control design for a multirotor UAV. *CEAS Aeronaut. J.* **2020**, *11*, 873–884. [CrossRef]

22. Bo, G.; Xin, L.; Hui, Z.; Ling, W. Quadrotor helicopter attitude control using cascade PID. In Proceedings of the 28th Chinese Control and Decision Conference, CCDC 2016, Yinchuan, China, 28–30 May 2016; pp. 5158–5163. [CrossRef]

23. Wang, P.; Man, Z.; Cao, Z.; Zheng, J.; Zhao, Y. Dynamics modelling and linear control of quadcopter. In Proceedings of the International Conference on Advanced Mechatronic Systems, ICAMechS, Melbourne, Australia, 30 November–3 December 2016; pp. 498–503. [CrossRef]

24. Rico-Azagra, J.; Gil-Martínez, M.; Rico, R.; Nájera, S.; Elvira, C. A benchmark for orientation control of a multirotor in a three degrees-of-freedom rotation structure. *Rev. Iberoam. Autom. Inform. Ind.* **2021**, *18*, 265–276. [CrossRef]

25. Hancer, M.; Bitirgen, R.; Bayezit, I. Designing 3-DOF Hardware-In-The-Loop Test Platform Controlling Multirotor Vehicles. *IFAC-PapersOnLine* **2018**, *51*, 119–124. [CrossRef]

26. Bajelani, M.; Tayefi, M.; Zhu, M. A real-test and simulation combined platform for developing intelligent tracking control of multirotors. *Int. J. Intell. Unmanned Syst.* 2022, *in press*. [CrossRef]

27. Chávez-Gudiño, M.A.; Concha-Sánchez, A.; Maciel-Barboza, F.M.; Gadi, S. K.; Thenozhi, S.; Jiménez Betancourt, R. Development and control of a low cost 2 DOF laboratory helicopter. *RIAI Rev. Iberoam. Autom. Inform. Ind.* 2023, *in press*. [CrossRef]

28. Ebeid, E.; Skriver, M.; Terkildsen, K.; Jensen, K.; Schultz, U. A survey of open-source UAV flight controllers and flight simulators. *Microprocess. Microsyst.* **2018**, *61*, 11–20. [CrossRef]

29. Gallarta-Sáenz, D.; Rico-Azagra, J.; Gil-Martínez, M. Learning Enhancement of Control Engineering: A Competition-Based Case. *IEEE Access* **2023**, *11*, 38240–38250. [CrossRef]

30. Control Engineering—Spanish Automatic Committee (CEA) and University of La Rioja Research Group. Competition: Orientation Control of a Multirotor—CIC2021. 2021. Available online: https://www.unirioja.es/dptos/die/cic2021/resultados.shtml (accessed on 16 July 2023).